

Formation of the Zn/CdTe(100) interface: Interdiffusion, segregation, and Cd-Zn exchange studied by photoemission

C. Heske, U. Winkler, D. Eich, R. Fink, and E. Umbach

Experimentelle Physik II, Universität Würzburg, Am Hubland, D-97074 Würzburg, Germany

Ch. Jung and P. R. Bressler

BESSY-GmbH, Lentzeallee 100, D-14195 Berlin, Germany

(Received 17 March 1997)

The interface formation of Zn/CdTe(100) has been investigated using synchrotron and Mg $K\alpha$ x-ray photoelectron spectroscopy. We identify five distinct phases of the interface formation process, including the passivation of surface defects by small amounts of adsorbed Zn ($\leq 0.1 \text{ \AA}$), diffusion of Zn into Cd vacancies and lattice-site defects, and a Cd-Zn exchange, thus forming the ternary compound $\text{Cd}_{1-x}\text{Zn}_x\text{Te}$ in a near-surface region. In the final stage of the interdiffusion, we find significant Cd segregation and also, to a smaller extent, Te segregation. The formation of a metallic Zn overlayer for high Zn coverages is associated with a surface photovoltage effect at room temperature. The results derived from the investigation of Zn-induced band bending, surface core-level shifts, and peak area evaluations are discussed, and a model based on the variation of the photoemission information depth is given. We also present a simple method to determine the onset of Cd segregation in order to identify the ternary $\text{Cd}_{1-x}\text{Zn}_x\text{Te}$ surface-alloy with maximum Zn content. [S0163-1829(97)01844-4]

I. INTRODUCTION

Among II-VI semiconductor compounds, CdTe plays a dominant role due to the wide field of its technological applications such as infrared detectors and solar cells. Employing ternary CdTe-based compounds such as $\text{Cd}_{1-x}\text{Zn}_x\text{Te}$, band-gap and/or lattice parameter engineering can be performed by a variation of the concentration parameter x . Thus lattice mismatch, generally encountered in the formation of semiconductor heterojunctions, can be minimized by choosing the appropriate ternary concentration, hence reducing the density of defects at the semiconductor interface. Moreover, band-gap engineering allows the design of special, problem-oriented band-offset structures to either minimize or maximize the influence of valence- and conduction-band offsets in semiconductor heterojunctions.

These engineering opportunities are generally approached from a "bulk point of view," i.e., by using ternary substrate materials or by growing thick, bulklike films by molecular beam epitaxy (MBE) or atomic layer epitaxy (ALE). However, the interface properties of a semiconductor heterojunction strongly depend on the *surface* properties of the underlying substrate material such as the ternary composition at the surface, the electronic and geometric surface structure, the surface band gap, the Fermi-level pinning position, and, in the case of polar surfaces, the surface termination.

Therefore, two different procedures appear feasible in order to gain a detailed understanding of heterojunctions involving ternary semiconductors. First, one could investigate the influence of variations of the bulk parameters on the surface properties, and thus establish rules which allow to derive indirectly the state of the surface from bulk operations. Or, second, one could generate the ternary compound in a near-surface region by interdiffusion of the third constituent into a binary substrate material, as was first pointed out by Wall *et al.* for Mn/CdTe(110).¹

In this study, we demonstrate the possibility of the second

approach in the case of Zn and CdTe(100) by investigating the electronic structure of the near-surface region, and by employing the dependence of the x-ray photoemission information depth on the energy of the incident photons. The installation of an additional Mg $K\alpha$ x-ray source at the PM5 (HE-PGM3) monochromator beamline at the BESSY storage ring enabled us to cover a wide photon energy range (1253.6 eV and 90–650 eV), combined with the high spectral resolution at high photon energies for the synchrotron experiments.² Thus the investigation of surface core-level shifts (SCLS's) of low-lying core levels such as Cd $3d$ and Te $3d$, and a comparison of core-level emission for various kinetic energies were possible. No photoemission investigations of Zn adsorption on II-VI semiconductors have hitherto been reported, to our knowledge.³

As will be discussed throughout the paper, the interdiffusion processes of the Zn/CdTe system take place in several distinct phases. However, we will present a simple method of determining the stage of interdiffusion by investigating the shift of core-level photoemission peaks, which provides a valuable monitor for the formation of $\text{Cd}_{1-x}\text{Zn}_x\text{Te}$ in the near-surface region.

In Secs. II and III, the experimental parameters and results will be presented. The analysis of Zn-induced core-level shifts and band bending as well as the information derived from Cd surface core-level shifts will be given in Sec. IV. Finally, Sec. V presents an interdiffusion model based on the experimental data and on a simple model calculation for the photoemission signal attenuation with increasing Zn coverage.

II. EXPERIMENT

The interface formation of Zn/CdTe(100) was studied by successively evaporating Zn from an Al_2O_3 crucible onto a commercial CdTe(100) single-crystal surface at a rate of approximately 1 \AA per minute. The polar (100) surface of the

CdTe substrate was prepared by repeated sputter (1-keV Ar ions) and annealing steps (300 °C). The validity of this approach and its influence on surface structure and termination have been thoroughly investigated, and are reported elsewhere.⁴⁻⁷ For the present preparation conditions the investigation of surface core-level shifts revealed a Cd-terminated surface.

We employed the high energy resolution of the plane grating monochromator PM5 (HE-PGM3) at the BESSY synchrotron source for a wide photon energy range using the HIRES photoemission spectrometer. At a photon energy of $h\nu=450$ eV, the Gaussian (i.e., total experimental), contribution to a Voigt line-shape fit of the Cd $3d_{3/2}$ core-level spectra is about 0.4 eV.

In studies using successive overlayer deposition steps, great care has to be taken to minimize the overall measurement time in order to avoid influences of contamination from residual gas particles (the base pressure in our experiments was 2×10^{-10} mbar). Even though no significant O $1s$ or C $1s$ photoemission signals could be detected at the end of a stepwise deposition series, we minimized possible contamination effects (such as the formation of ZnO) by investigating two separate deposition series, with an emphasis on different experimental information. In the first series, the surface structure of the pristine CdTe substrate alone was monitored by low-energy electron diffraction (LEED), and the synchrotron photoemission investigations after each deposition step focused on the valence-band region and the (shallow) core levels Cd $4d$, Te $4d$, Zn $3d$, and Zn $3p$. In addition, Mg $K\alpha$ x-ray photoemission spectroscopy (XPS) measurements of each element were performed in order to allow a comparison of results from different information depths. For the second series, the attention was aimed at a LEED investigation after each deposition step and at the investigation of the SCLS's of the Cd and Te $3d_{3/2}$ levels in addition to the above-mentioned (shallow) core-level measurements. No Mg $K\alpha$ measurements were performed in this case. The LEED investigations revealed an unreconstructed surface [(1×1) LEED pattern] for the pristine CdTe sample in both series. The surface structure did not change with increasing Zn coverage up to a nominal coverage of 14 Å (second series), while the background intensity of the LEED pattern increased. Above 14 Å, no LEED pattern could be observed.

The thickness determination of deposited Zn overlayers is a rather problematic task, for two reasons. First, Zn deposition leads to a significant diffusion into the substrate material, e.g., CdTe, as will be shown below. Second, Zn appears to have a rather small sticking coefficient on some surfaces, which is consistent with the extremely high Zn vapor pressure required for detailed-balance conditions.⁸ We also noticed severe problems when determining the Zn overlayer thickness by using a quartz microbalance which monitored the Zn flux at the sample position before and after each deposition step. In a first deposition series the microbalance quartz was covered with a thick CdTe overlayer, while the quartz had to be replaced before a second deposition series. On the clean quartz surface the sticking coefficient was drastically enhanced (by about a factor of 4), and hence much larger fluxes were monitored. Therefore, we had to renormalize the exposure of the second series such that a consistent

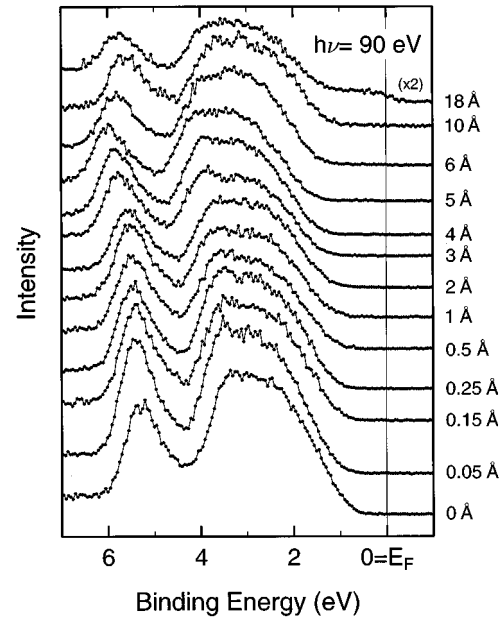


FIG. 1. Photoemission spectra ($h\nu=90$ eV) of the upper valence-band region of CdTe(100) (0-Å Zn) and for different nominal Zn coverages. The first evidence of a Fermi edge (i.e., for a metallic overlayer) is detected in the 18-Å spectrum. The Fermi energy of the instrument and hence the binding-energy scale was separately determined by a sputter-cleaned Au-foil reference. The spectra were normalized by the background count rate on the high-binding-energy side.

quantitative development of all data occurred. It is noted that the determination of the Zn overlayer thickness may generally be quite uncertain, and that the thicknesses given in this paper are just nominal values which are accurate as relative measure within a series but not as absolute values.

III. PHOTOEMISSION SPECTRA

The evolution of the upper valence band region of CdTe is shown in Fig. 1 for increasing Zn coverage. While no significant changes in the overall spectral shape are detected, both the valence-band edge as well as the (partly angle-integrated) split-off band at a binding energy between 5 and 6 eV experience a downward shift toward higher binding energies up to a nominal Zn coverage of 5 Å (for a detailed discussion of the valence region emission features of CdTe we refer to Refs. 9–17). For higher coverages (6 and 10 Å), an upward shift of the spectral features is observed. At 18 Å, finally, a Fermi edge is resolved, suggesting the formation either of a metallic Zn overlayer or of sufficiently large Zn islands. The position of the Zn Fermi edge is detected at a slightly higher kinetic energy (0.15 eV) than the Fermi energy of the instrument as derived from a sputter-cleaned Au reference. This effect is due to a surface photovoltage (SPV) frequently encountered in metal-semiconductor investigations with synchrotron photoemission.^{18,19} Even at room temperature such a surface photovoltage can be detected, e.g., for the Mn/Cd(Zn)Te(100) interface system.²⁰ In the case of Zn/CdTe, the largest SPV effect we observed at room temperature is a 0.3 eV shift toward higher kinetic energies,

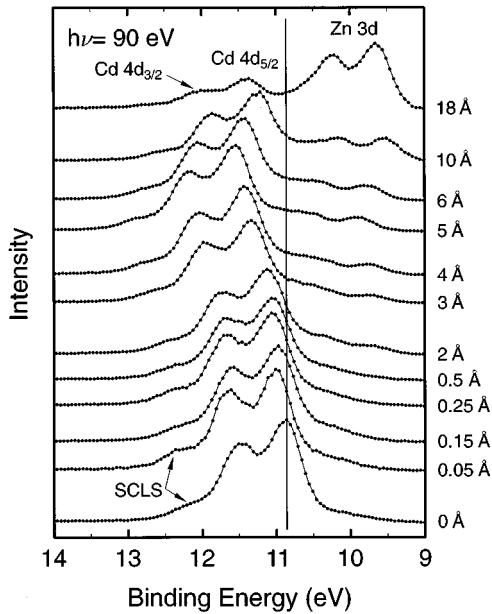


FIG. 2. Photoemission spectra ($h\nu=90$ eV) of the lower valence-band region of CdTe(100) for increasing nominal Zn coverages, showing the spin-orbit-split Cd 4d features (at about 10.9 and 11.5 eV in the 0-Å Zn spectrum) and their surface-shifted components at higher binding energy (labeled SCLS) as well as two Zn 3d emission features (9.7 and 10.2 eV in the 18-Å spectrum) which appear for nominal coverages ≥ 2 Å. The spectra were normalized by the count rate average of the high- and low-binding-energy sides.

as is in accordance with the overall downward band bending in Fig. 1.

The lower valence-band region of CdTe(100) and the Zn/CdTe interface is shown in Fig. 2. The displayed spectral features are superpositions of several shallow core levels: the dominant feature in the lowest spectrum (0-Å Zn) is mainly composed of the spin-orbit-split Cd 4d core level (at about 10.9 and 11.5 eV). Moreover, Cd atoms located in the top-most layer of the polar (100) surface give rise to a SCLS which is mainly due to a change of the coordination state, the Madelung potential, the cation-anion charge transfer, and/or the final-state screening of the photo hole.⁷ As will be discussed in more detail in Sec. IV, this surface-shifted component of the Cd 4d_{3/2} level is detected on the high-binding-energy side of the bulk peak, and thus leads to a shoulder between 12 and 12.5 eV in the bottom spectra. Furthermore, dispersing Te 5s emission²¹ and transitions from the X_6^v critical point¹² have been reported on the low-binding-energy side of the Cd 4d bulk peaks.

As in the case of the upper valence-band region, a downward band bending (i.e., a shift toward higher binding energies) is observed in Fig. 2 for the composed Cd 4d feature with increasing Zn coverage up to 5 Å, followed by an upward shift for further deposition steps and a downward shift for the highest Zn coverage (for which a Fermi edge is resolved). Apart from an influence on the SCLS to be discussed in Sec. IV no significant line-shape changes of the Cd 4d emission are detected for increasing Zn coverage.

Finally, additional emission features pertaining to the Zn 3d levels evolve around a binding energy of 10 eV with

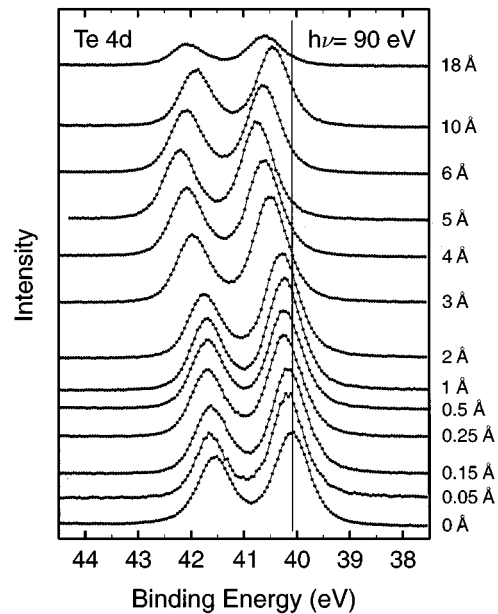


FIG. 3. Photoemission spectra of the Te 4d levels of CdTe(100) for increasing nominal Zn coverages ($h\nu=90$ eV). The spectra were normalized by the count rate average of the high- and low-binding-energy sides.

increasing Zn coverage. Two clearly distinct peaks separated by 0.6 eV can be detected at and above a nominal Zn thickness of 2 Å.

A large number of values has been reported for the magnitude of the spin-orbit splitting of the Zn 3d levels, varying from zero to almost 0.8 eV.²²⁻²⁶ For the Zn(0001) surface, Himpsel *et al.* emphasized the band character of the Zn 3d states in finding that their observations such as energy dispersion and interband transitions are incompatible with an atomic core-level model.²⁷ Similarly, Wei and Zunger clarified the role of the Zn 3d states in II-VI semiconductors, finding that *p-d* repulsion and hybridization have some influence on the semiconductor properties, among others on the magnitude of the spin-orbit splitting.²⁸

Based on our experimental results, we believe that the Zn 3d emission features have to be viewed in the context of a band structure rather than as pertaining to atomic core-level emission. Thus, the two peaks are interpreted as being due to spin-orbit splitting *in conjunction* with hybridization and delocalization. The coexistence of two different Zn species seems unlikely, since the intensity ratio of the two Zn 3d peaks remains approximately constant throughout the whole deposition series. We indeed detect two different Zn species, as will be discussed below (Fig. 4), but the first species is found for the first Zn deposition steps, while the second species evolves at a nominal thickness of 1 Å, comparable to the coverage range in which the Zn 3d emission features appear. Apparently, the discernible Zn 3d features are associated only with the second Zn species, which suggests a strong interaction of the first Zn species with the CdTe substrate, and a strong Zn 3d contribution to the chemical bond by mixing with valence orbitals (bands).

In Fig. 3 the photoemission spectra of the Te 4d core levels are shown. As in the case of Cd, no significant changes in line shape are detected, thus giving no evidence

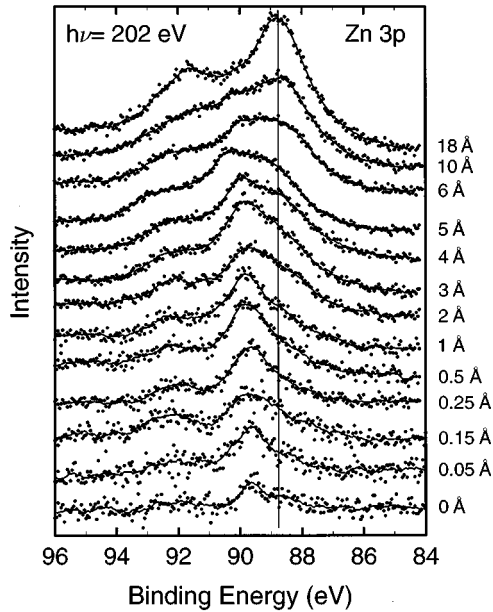


FIG. 4. Zn $3p$ photoemission spectra taken at $h\nu=202$ eV. Some Zn emission can be detected even for the nominally Zn-free CdTe single crystal surface (0-Å Zn spectrum). With increasing Zn coverage, a second Zn species at lower binding energy can be distinguished (nominal coverage ≥ 1 Å), which becomes dominant in the high-coverage regime. The spectra were normalized by the count rate at the low-binding-energy side.

for the formation of a second Te species (e.g., ZnTe). The peak positions of the Te $4d$ core levels are also shifted toward higher binding energies with increasing Zn coverage, reaching a maximum at 5 Å, and are shifted back for higher coverages. Again, the spectrum with the metallic overlayer (18-Å Zn) reveals a line position at higher binding energy.

The Zn $3p$ spectra of Fig. 4 taken from the second sample exhibit a small Zn signal even for the pristine, nominally Zn-free CdTe surface (in contrast to the first sample, which showed no Zn signal). At this point, the sample had merely been sputtered and annealed in the photoemission chamber, and had *not* yet been transferred into the MBE chamber; a contamination of the surface from the Zn source can thus be ruled out. We therefore expect this line position to be representative of the substitutionally incorporated Zn in $\text{Cd}_{1-x}\text{Zn}_x\text{Te}$.²⁹ For increasing Zn coverage, the same binding-energy shift of all spectral features as in the Cd and Te case is detected. Moreover, a second Zn species at lower binding energy evolves at a nominal coverage of 1–2 Å, in coincidence with the above-mentioned detection of the Zn $3d$ double peak of Fig. 2. This second phase becomes dominant in the high-coverage (18 Å) spectra, and is thus considered to represent Zn atoms in a metallic or nonionic bonding state.

From Zn $2p_{3/2}$ XPS spectra taken with Mg $K\alpha$ radiation (not shown), the same behavior can be derived as for synchrotron measurements of the Zn $3p$ levels. In this case the line position of the first few deposition steps is significantly shifted toward lower binding energy, and the linewidth is increased with increasing nominal coverage ≥ 1 Å due to a superposition of the two Zn species. For high coverages, large amounts of Zn are detected, which can be significantly

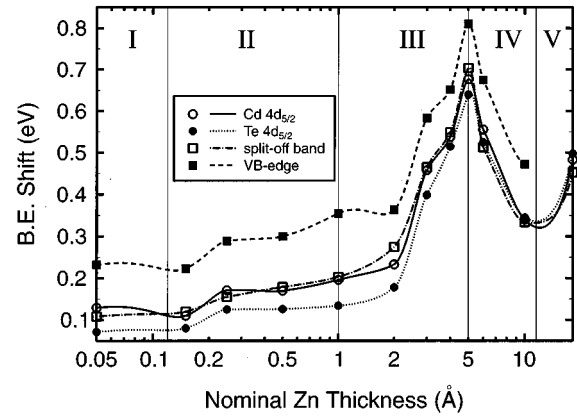


FIG. 5. Binding-energy shifts of various photoemission features with respect to the binding energies of pristine CdTe (i.e., 0-Å Zn) for increasing nominal Zn coverage on a logarithmic scale. The open squares pertain to the split-off band at a binding energy of 5–6 eV (see Fig. 1). The edge of the valence band (full squares) was determined by linear extrapolation. The various interdiffusion phases (I–V) are discussed in the text.

reduced by annealing at 300 °C in UHV for 10 min. Apparently, a large amount of Zn atoms can be removed from the photoemission information volume via desorption and/or diffusion into the bulk.

Several general trends can be derived from the experimental results presented so far. First, a prominent Zn diffusion is expected from the fact that a Zn Fermi edge is detected only at very high nominal coverages, while the Zn $2p$, $3p$, and $4d$ spectra reveal significant amounts of Zn within the photoemission information volume. Second, two different Zn species are detected, which can be correlated with substitutionally incorporated Zn at low nominal coverages, and with Zn in a nonionic or metallic environment in the high-coverage range. Finally, a relatively complex band-bending behavior has been observed for increasing Zn coverage. From these results we derive several distinct interdiffusion phases for the Zn/CdTe interface formation, which will be discussed in the following sections.

IV. EVALUATION OF BINDING-ENERGY SHIFTS

In this section, a more detailed analysis of the binding-energy shifts with increasing Zn coverage will be given, and we take a closer look at the surface core-level shifts revealing the surface termination. The results of this analysis then lead to the model presented in Sec. V.

In Fig. 5 the binding-energy shifts of several photoemission signals are displayed for increasing Zn coverage. The values are referred to those from the pristine, unexposed CdTe(100) surface (0-Å Zn, and a binding energy shift of 0 eV, not shown due to the logarithmic scale of the abscissa). The data points have all been derived from photoemission spectra taken at $h\nu=90$ eV, which gives the maximal photon energy resolution for fixed settings of monochromator slits and electron analyzer parameters. Great care was taken to determine the position of the Fermi energy of the instrument with a Au-foil reference for each injection of the BESSY storage ring. Throughout the deposition series, the photon

energy (and thus the measurement of the Fermi energy) varied by less than 0.04 eV.

Apart from the Te $4d_{5/2}$ and the bulk Cd $4d_{5/2}$ peaks, the split-off band at a binding energy between 5 and 6 eV (see Fig. 1) and the valence-band edge have been evaluated. The position of the edge has been determined by a linear extrapolation. Since no significant changes in the shape of the valence-band edge occurred during the Zn deposition steps, this procedure is regarded as exact (within ± 0.1 eV) in determining relative energy shifts such as those presented in Fig. 5.

The band-bending behavior of the Zn/CdTe interface formation can be divided into five different phases. The first phase consists of the pristine CdTe and the very first deposition step, and will be discussed in more detail below. In a second phase (II), the energy position of all evaluated spectral features remains moderately constant, while there is a sharp increase of the binding energy in the third phase (III), reaching a maximum for a nominal Zn thickness of 5 Å. Note that the onset of the third phase coincides with the first detection of the second Zn species and the evolution of the Zn $3d$ emission features. The two final phases (IV and V) are characterized by the beginning formation of a metallic overlayer. In phase IV no Fermi edge of the Zn overlayer can yet be detected, in contrast to phase V, where a Fermi edge is clearly visible in the valence-band region. In view of the growth start of the metallic Zn overlayer, we thus tentatively assign phase IV to the existence of small Zn islands or clusters. The distinction between phases IV and V, however, is somewhat arbitrary, since it relies on the sensitivity of the photoemission measurements such as the surface density of states at the Fermi edge or the photoemission matrix element, and on the critical cluster size for the formation of a Fermi edge.

As mentioned above, we detect a surface photovoltage effect once a Fermi edge is present in the valence region spectra (phase V). In our case, the correction of this effect leads to an increase in binding-energy shift of all spectral features, i.e., to an upward shift in Fig. 5. Moreover, we expect such a SPV effect to play an important role also in phase IV, in which the formation of the metal-semiconductor interface begins, even though no Fermi edge is yet detected with photoemission due to the low cross section of Zn $4s$ states. Since, in phase V, the SPV effect decreases in magnitude for increasing Zn coverage, we expect the correction in phase IV to be even larger. Thus, we believe that the downward ‘‘bowing’’ in phases IV and V of Fig. 5 can be understood qualitatively on the basis of the SPV effect.

We now come back to the discussion of phase I, which comprises the pristine CdTe(100) surface and the very first deposition step. Phase I is displayed together with phase II in Fig. 6 on a linear scale (lines are intended as guide to the eye). As can clearly be derived from Fig. 6, there is a pronounced difference between the binding-energy shift of the valence-band edge and those of all other investigated features, which is established in the very first Zn deposition step. Note that the errors for the binding-energy determination are estimated to be 0.05 and 0.1 eV for the photoemission peaks and the valence-band edge, respectively, so that the three emission features are equal within the error bars, while the difference between the valence-band edge and

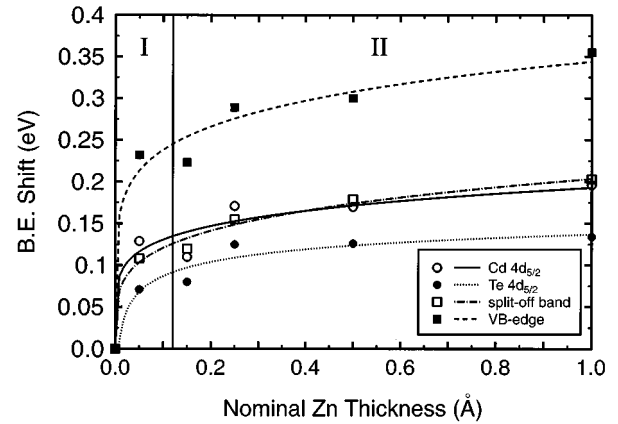


FIG. 6. Enlarged view of the binding-energy shifts of Fig. 7 for the first few deposition steps on linear coverage scale (phases I and II). The lines were determined by a least-square fit and are intended as a guide to the eye. A significantly larger binding-energy shift of the valence band edge as compared to all other spectral features is established in the very first deposition step.

those three features cannot be explained solely by determination errors.

Which origins could account for a difference in the band bending of different photoemission spectral features? In principle, a surface band bending induced by surface states or adsorbate atoms is expected to alter the local electronic potential, and will thus affect all spectral features equally. An influence of final-state effects can be ruled out, since one would have to assume a better screening of the photo hole for the core levels than for the valence-band maximum. An explanation based on the increase in band gap due to the formation of a ternary $\text{Cd}_{1-x}\text{Zn}_x\text{Te}$ compound also appears unlikely, because of the small amounts of Zn deposited during the first deposition step.

We favor a different explanation for the enhanced downward shift of the valence-band (VB) edge, which is the saturation of surface defects or quenching of surface states which are located just above the VB edge by adsorbed Zn atoms. It was pointed out by Gawlik and co-workers^{15,16} for the (1×1) -unreconstructed CdTe(100) surface that the top of the valence band at the Γ point consists of a surface resonance superposed onto the bulk band structure. For certain k -space directions, surface states are detected above the valence band. This surface resonance could be visible in the spectrum of the pristine surface, and could be rapidly quenched by small amounts of Zn. In addition, surface defects, such as Cd and Te surface vacancies, terrace steps, and dislocations, may also contribute to the surface density of states at and above the actual valence-band edge. In our case, the mere existence of a (1×1) -unreconstructed surface gives some evidence for an imperfect distribution of unsaturated bonds, which can be related to an increased density of surface defects. Moreover, the downward shift of *all* emission features after the first deposition step can be interpreted as a change of the Fermi-level pinning position due to a saturation of surface defects or a quenching of the surface resonance. Thus it appears very likely that the adsorbed Zn atoms in the very first deposition step primarily influence the surface resonance and/or defects, leading to a reduced surface density of states

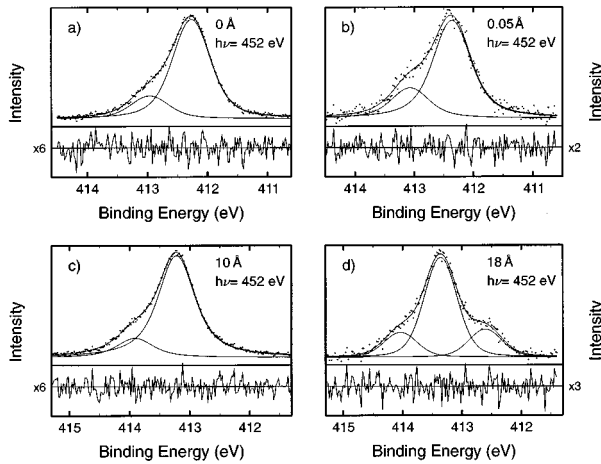


FIG. 7. Photoemission spectra of the Cd $3d_{3/2}$ core levels for the pristine CdTe(100) surface (a), after the first Zn deposition step (b), and for high nominal Zn coverages [(c) 10 Å and (d) 18 Å]. Below each spectrum the residual, i.e., the difference between the measurement and the Voigt line shape fit is shown.

at and above the valence-band maximum; this causes the increased shift of the “VB edge.” The fact that the edge shape is not changed upon this shift is not surprising if the magnitude of the shift, the experimental resolution, and the probably broad spectral distribution of such states are considered.

The explanation of a surface defect saturation or surface resonance quenching by adsorbed Zn atoms in the very first deposition step is corroborated by an investigation of the SCLS’s of the topmost Cd atoms. Figure 7 shows the Cd $3d_{3/2}$ core levels for the pristine CdTe(100) surface (a), after the first Zn deposition step (b), and for high nominal Zn coverages [(c): 10 Å and (d): 18 Å]. As discussed above for the Cd $4d$ levels, a SCLS is detected as a shoulder at the high-binding-energy side. Since no SCLS is found for the Te $3d_{3/2}$ level (not shown), we conclude a Cd termination of this surface, in accordance with earlier results.^{5,7} The relative intensity of the surface-shifted component was increased by choosing the photon energy such as to maximize the surface sensitivity.⁷ Contrary to what one would expect for the relative surface intensity upon deposition of adsorbate atoms, the Cd surface-shifted component *increases* after the first Zn deposition step (the surface-to-bulk area ratio increases significantly from 0.23 to 0.31). For further deposition steps, the relative surface intensity does indeed decrease, as expected. This finding is in accordance with the idea of passivation of surface defects by adsorbed Zn atoms in the very first deposition step, leading to a more homogeneous potential distribution at and within the surface top layer. Thus more Cd atoms are embedded in an environment characteristic of the surface-shifted emission features in Fig. 7. For example, a Cd vacancy in the top layer will reduce the Madelung potential for all neighboring Cd atoms. This will lead to a shift toward smaller binding energy, i.e., toward the bulk position. The passivation of the Cd vacancy by a Zn atom will reverse this shift, and hence an increased surface component will be detected [Fig. 7 (b)]. Furthermore, a Cd vacancy will also alter the electronic state of neighboring Te atoms in the second layer, and hence also indirectly influence the neighbor-

ing Cd atoms in the top layer. Again, this influence would lead to a shift towards the bulk position, and is reversed for the passivation of the Cd vacancy by a Zn atom. It is emphasized that the relative intensity of the SCLS-shifted component is hence a direct measure of the quality and homogeneity of the topmost surface layer.

As stated above, the surface-shifted component decreases with increasing Zn coverage, but nevertheless remains present, as can be seen in Fig. 7(c) for the 10-Å spectrum. Conversely, no Te SCLS is detected throughout the whole deposition series. Apparently the Cd termination is not abolished in the interdiffusion and interface formation processes. Once the metallic Zn overlayer is established and a Zn Fermi edge can be detected, a third Cd species at lower binding energy (0.75 eV with respect to the bulk Cd emission from CdTe) can be detected, as shown in Fig. 7(d) for a nominal Zn thickness of 18 Å. Three possible origins of this third species are feasible: First, this species pertains to emission from Cd in an interfacial layer between the (interdiffused and Cd-“terminated”) Cd(Zn)Te semiconductor and the metallic Zn overlayer. Second, Cd can be dissolved in the growing Zn film, either forming an intermetallic compound [as is known for Cd concentrations up to 1.17% (Ref. 30)] or an alloy. Finally, of course, segregation of Cd and enrichment on the surface of the Zn overlayer can be expected. Even though none of these three interpretations can be completely ruled out on the basis of our experimental results,³¹ we favor the third explanation, since we detect a strong enhancement of the Cd signal in surface sensitive measurements as compared to bulk measurements for the 18-Å Zn deposition step; this will be discussed in more detail in Sec. V. Note that the surface-shifted Cd component can still be detected in the high-coverage spectrum, which is ascribed to emission from Cd atoms at the Zn/Cd(Zn)Te interface. This component is enhanced with respect to the bulk signal, while the overall intensity of the Cd $3d_{3/2}$ peaks is significantly reduced. These findings are consistent with the assumption that the Cd atoms at the interface exhibit a similar peak position as the previous surface atoms.

In Fig. 8, the evaluation of the Cd surface core-level shifts is presented on a logarithmic Zn coverage scale. The solid line (intended as guide to the eye), full dots, and the left ordinate pertain to the surface-to-bulk peak area ratio of the Cd $3d_{3/2}$ spectra. This is consistent with the substitution of Cd atoms by Zn in the surface (or interface) layer (and an additional indiffusion of Zn atoms), that the SCLS ratio decreases with increasing Zn coverage in the range of 0.05–10 Å. Note that this behavior cannot be explained only by the formation of a closed or partial Zn overlayer, since both signals would be attenuated by the same factor (this factor depends solely on the attenuation length of photoelectrons within the overlayer, which is identical for both signals under consideration). The SCLS remains approximately constant for all coverages (open squares, dotted line and right ordinate). At this stage of the analysis, we have identified several different phases of the Zn/CdTe interface formation which will be further discussed in Sec. V.

V. A PHASE MODEL FOR THE Zn/CdTe INTERFACE FORMATION

A. Interpretation of experimental results

This section is aimed at a further clarification of the Zn interdiffusion behavior during each phase of the Zn/CdTe

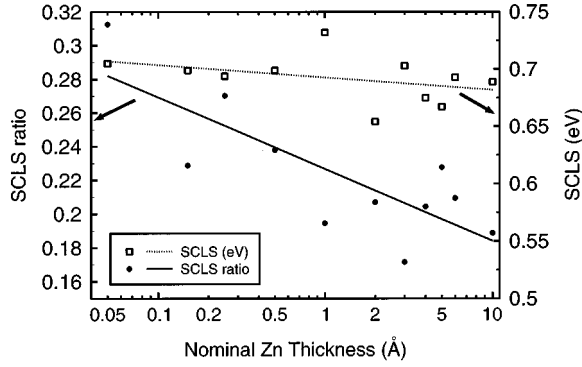


FIG. 8. Evaluation of the surface core-level shift (SCLS) data as derived from the Cd $4d_{3/2}$ core-level spectra. The solid line and full circles pertain to the SCLS ratio (i.e., the peak area ratio of the surface to bulk contributions), the dashed line and open squares represent the SCLS itself (i.e., the binding-energy difference between the two components). No significant trends are observed in the latter case, while the SCLS ratio decreases with increasing Zn coverage. The straight lines were determined by a least-square fit, and are merely intended as guides to the eye.

interface formation. In the data and interpretations given so far, we have neglected the quantitative analysis of the photoemission spectra. This has also been done by investigating the peak areas of all spectral features obtained in the first deposition series.

A quantitative analysis of peak areas from well-ordered surfaces can strongly depend on photoelectron diffraction (PED) effects. In fact, we have observed significant peak area variations for the Te $3d_{5/2}$ core level of a Cd-terminated, $c(2 \times 2)$ -reconstructed Cd(Zn)Te surface upon variation of the photon energy.²⁰ Since nearly no PED effects were observed for the Cd $3d_{5/2}$ core level, and since the PED effects for Te become negligible for kinetic energies above 65 eV, most of the peaks investigated in this study will not be significantly affected by PED effects. Although some influence on the results from the synchrotron measurements of Te and Cd $4d$ levels cannot be ruled out, the overall trends to be discussed in this section will nevertheless remain valid.

The normalized peak areas of the various photoemission peaks are presented in Fig. 9. The normalization of Cd and Te peaks was performed by dividing the peak area at each Zn deposition step by the value for the pristine CdTe surface, thus obtaining a ‘‘relative intensity.’’ The relative intensities for the Cd and Te peaks at a nominal Zn thickness of 0 Å are therefore equal to unity. Analogously, the Zn peaks were normalized by the peak area at the maximal nominal Zn thickness (i.e., at 35 Å); the normalized Zn areas at 0-Å Zn are zero. Open symbols represent the synchrotron photoemission results obtained for $h\nu=90$ eV, while filled symbols refer to the Mg $K\alpha$ XPS measurements. Cd levels are denoted by circles ($4d$ and $3d_{3/2}$, respectively), Te levels by squares ($4d$ and $3d_{3/2}$), and Zn levels by triangles ($3p$ and $2p_{3/2}$). Employing a wide range of different photon energies, the kinetic energies of the investigated photoelectron signals and hence their information depth could be varied. Table I gives an overview of the kinetic energies used and the associated electron inelastic mean free paths (IMFP’s) derived from the universal curve given by Seah and Dench,³² which

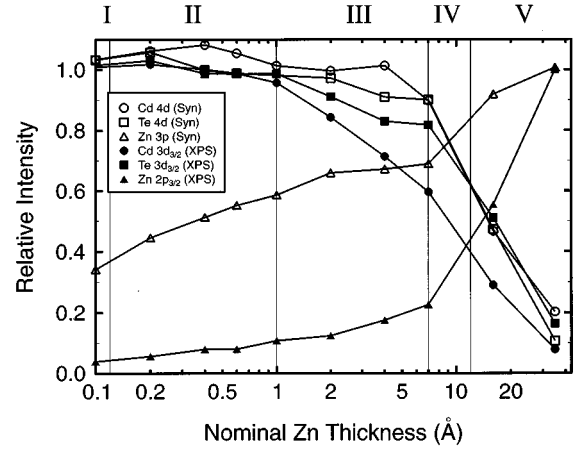


FIG. 9. The development of the relative intensities of the various Cd, Te, and Zn photoemission peaks as function of Zn coverage in a semilogarithmic plot (first series). Open symbols represent synchrotron photoemission measurements with higher surface sensitivity as compared to Mg $K\alpha$ XPS measurements (full symbols). The normalization was performed by dividing each data point by the corresponding value at 0-Å Zn for Cd and Te or at 35 Å for Zn. The various interdiffusion phases (I–V) are discussed in the text.

are in good qualitative agreement with recent, more accurate results published by Powell³³ and Gries.³⁴ The validity of the IMFP dependence on the kinetic energy given by Seah and Dench has been confirmed in case of ZnSe(100) in Ref. 35.

Figure 9 is subdivided into five different phases like Fig. 5. During the first phase we find a significant intensity increase of the surface sensitive Zn $3p$ signal from 0 to 0.33, while all other relative intensities remain close to their initial value for the pristine surface. This is derived from the values at 0.1 Å and those at 0 Å, which are 0 for Zn and 1 for Cd and Te. The error bar for the peak area determination is approximately $\pm 5\%$, leading to an error bar for the relative intensities of $\pm 7\%$. The significant increase in relative intensity of the surface-sensitive Zn signal corroborates the idea of a Zn-induced saturation of surface defects within the very first deposition step.

In the second phase, all relative intensities of Cd and Te remain close to unity, while there is a significant increase in the Zn signals, in particular in the surface-sensitive synchrotron measurements of the $3p$ signal. Apparently, the deposition of Zn does not significantly reduce the emission from the substrate peaks. This is again compatible with a partial

TABLE I. Kinetic energies of the photoelectron peaks contained in Fig. 9, along with their corresponding inelastic mean free paths (IMFP’s), according to Seah and Dench (Ref. 32).

Peak	$h\nu$ (eV)	E_{kin} (eV)	IMFP (Å)
Cd $3d_{3/2}$	1253.6	843	15.7
Cd $4d$	90	79.0	5.0
Te $3d_{3/2}$	1253.6	671	14.0
Te $4d$	90	48.5	4.4
Zn $2p_{3/2}$	1253.6	232	8.3
Zn $3p$	202	110	5.8

indiffusion of Zn, and rules out the formation of a Zn overlayer. At this stage, a discussion of possible indiffusion paths appears appropriate. First, Zn is expected to migrate along paths of increased bulk defect density (in particular Cd vacancies). Second, a migration along interstitial sites is possible, as reported for Ag in CdTe (Ref. 36) and Zn in $\text{Al}_x\text{Ga}_{1-x}\text{As}$ superlattices.³⁷ For Zn in InP, an interstitial-substitutional diffusion mechanism was derived,³⁸ while Zn is stable on an interstitial site of ZnSe up to 260 K.³⁹ Finally, an exchange mechanism of Zn and Cd has to be considered as well. In this case the released Cd atoms could be desorbed, could migrate into the bulk (i.e., leave the photoemission information volume), segregate at the surface, or diffuse by occupying lattice defects (particularly Cd vacancies) or interstitial lattice sites, as reported for Ag in CdTe.⁴⁰ These alternatives and their influences on the photoemission signals of both surface- and bulk-sensitive measurements have to be addressed by the model to be presented below. At this stage we would merely like to mention that in the second phase of Zn/CdTe interface formation (II), we expect a dominance of the Cd-Zn exchange within the photoemission information volume, thus detecting a Zn chemical state equal to substitutional Zn in $\text{Cd}_{1-x}\text{Zn}_x\text{Te}$ for the Zn 3*p* spectra in Fig. 4 (i.e., the first Zn species). This leads to an increase in both Zn signals, as derived from Fig. 9; moreover, we expect the Cd atoms to remain within the information volume either at lattice defects or on interstitial lattice sites, thus showing no significant variations of both Cd signals.

In contrast to phase II, in phase III we detect a significant difference in the relative intensities for the Cd signals. In this phase, the second Zn species appears in the Zn 3*p* spectra, which we have correlated with a more metallic chemical state of the Zn atoms. Thus the following description for the third phase is favored: freshly deposited Zn atoms continuously diffuse into the CdTe bulk region. Some Cd atoms on lattice sites are still replaced by Zn, while an increasing number of Zn atoms also occupies interstitial and defect sites (the second Zn species), forcing the Cd atoms to migrate into the bulk of the sample (thus leaving the information volume of our experiment) and to the surface. Moreover, the (local) lattice parameter is expected to decrease upon the exchange of Cd by Zn on a regular lattice site, so that the Cd atoms are forced away from the contracted area (again into the bulk or to the surface). Accordingly, we find a significantly larger decrease in the XPS measurements of Cd as compared to the surface-sensitive synchrotron results, as would be expected for a surface segregation and a migration into the bulk beyond the photoemission information depth.⁴¹ The suggestion of surface segregation is supported by the fact that no LEED pattern was observed for nominal Zn coverages above 3 Å.

Phases IV and V have already been assigned to the existence of metallic Zn clusters or islands (phase IV) and the formation of a metallic Zn overlayer (phase V). As would be expected for such a picture, the relative intensities of the substrate signals are decreased, while the relative intensities of Zn (forming the overlayer) are increased.

In order to gain more insight into the quantitative behavior of the relative intensities for increasing nominal Zn thickness, we employed a simple model of exponential attenuation of the photoemission signal with increasing emitter depth relative to the surface. The first step was to plot the

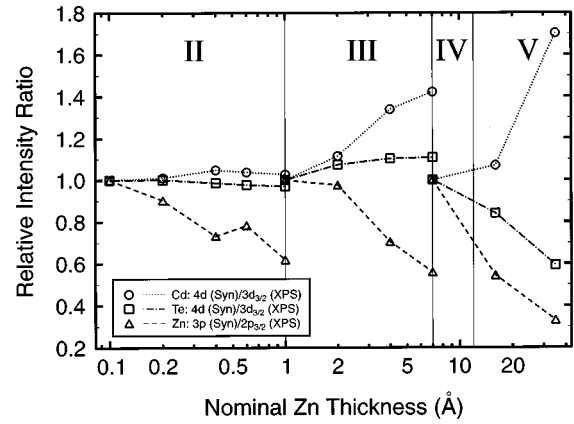


FIG. 10. Relative Cd, Te, and Zn photoemission peak intensity ratios as function of Zn coverage on a semilogarithmic scale (first series), normalized by the corresponding start coverage of each interdiffusion phase. The relative intensity ratio for each element was formed by dividing the normalized relative intensity of the surface-sensitive synchrotron measurement by the corresponding bulk-sensitive XPS data. The various interdiffusion phases (II–V) are discussed in the text.

data presented in Fig. 9 in an alternative way (Fig. 10). Here, the normalization was performed separately for each phase, by dividing the photoemission peak areas of the corresponding emission features by their value for the lowest nominal Zn coverage of that particular phase. For example, all emission intensities of phase III were normalized by their respective value at a nominal Zn thickness of 1 Å. Moreover, we divided the relative intensity ratio of the synchrotron measurements (with high surface sensitivity) by the corresponding XPS value (with lower surface sensitivity), thus forming a relative intensity ratio (RIR). An increase in the RIR with increasing nominal Zn thickness will therefore represent a relative enhancement of the surface signal as compared to the bulk signal. Based on the error for peak area determination of 5% a relative error of 10% is derived for the RIR values.

Is our interdiffusion model compatible with Fig. 10? The starting point of phase II is, according to our model, the pristine CdTe surface, with some Zn atoms passivating the surface defects of the substrate. Thus, the normalization of the Zn RIR of phase II is performed with a sample state of Zn atoms primarily located in the first monolayer (note that the data in Figs. 9 and 10 pertain to the first series, where no Zn was found in the pristine CdTe substrate). With increasing nominal thickness, some Zn atoms are adsorbed on the surface, but significantly more atoms diffuse into the near-surface bulk region, therefore enhancing the bulk-sensitive signal more strongly, and reducing the Zn RIR in phase II as well as in all other phases (III–V). The Cd and Te RIR remain close to unity in phase II. Assuming a homogeneous distribution of Cd and Te atoms at a nominal Zn thickness of 0.1 Å, this can be associated with a homogeneous distribution throughout phase II as well. In phase III, however, we derive a marked difference for Cd and Te: while the Te RIR stays close to unity again, the Cd RIR increases significantly, revealing an enhancement of the surface-sensitive signal as

compared to the bulk-sensitive case. This finding supports the idea of a Cd surface segregation during phase III.

According to our model, phases IV and V are dominated by the formation of metallic Zn clusters and islands, leading to the formation of a metal Zn overlayer with a detectable Fermi edge. In this case, a reduction of the Cd and Te RIR would be expected, since the information depth of the surface-sensitive measurements is more and more occupied by Zn atoms in the overlayer, thus reducing the relative intensity of the synchrotron measurements with respect to the XPS measurements. This behavior can be found for the Te RIR, while the Cd RIR increases significantly at the last deposition step. In this case, as already discussed in conjunction with SCLS investigations, we find a third Cd species, which is, in view of the increased RIR, attributed to a segregated species on top of the growing metallic Zn overlayer. The decrease of the Zn RIR suggests that a significant amount of Zn atoms still diffuses into the semiconductor bulk.

B. Calculations

In order to support the described model further, we performed calculations based on an exponential dependence⁴² of the photoemission intensity on the emitter position z , the attenuation length $\lambda_M(E_X)$ of photoelectrons of element X with kinetic energy E_X in the crystal matrix M , and on the atomic densities $N_X(z)$, X being Cd, Te, or Zn. We assumed normal emission (as in our experiment), and summarized ionization cross sections, spectrometer terms, and lateral variations into a normalization term I_X^0 , thus arriving at an expression for the photoelectron intensity for a kinetic energy E_X :

$$I_X(E_X) = I_X^0 \int_0^\infty N_X(z) \exp[-z/\lambda_M(E_X)] dz. \quad (1)$$

Comparing the results of our calculations with Fig. 10, we have to form the RIR for two different kinetic energies E_X^1 and E_X^2 and for both, the nominal Zn thickness s and its reference value s_{ref} (i.e., 0.1 Å in phase II and 1 Å in phase III):

$$\text{RIR} = \frac{I_X(E_X^1, s)/I_X(E_X^1, s_{\text{ref}})}{I_X(E_X^2, s)/I_X(E_X^2, s_{\text{ref}})}. \quad (2)$$

Note that, upon evaluating Eq. (2), the I_X^0 normalization terms are canceled, thus eliminating any dependence of the RIR on photoemission cross sections and spectrometer terms. Moreover, normalization factors for the atomic densities N_X are canceled as well, so that we could employ as convenient parametrization the relative atomic densities with respect to the pristine CdTe sample. Thus the atomic density of Cd is 1 for CdTe, 2 for a pure Cd overlayer, and $1-x$ when a fraction of x Cd atoms is replaced by Zn atoms. Accordingly, the atomic density of Zn is also related to the Cd density in pristine CdTe, therefore assigning $N_{\text{Zn}}=1$ to a pure ZnTe sample, $N_{\text{Zn}}=2$ to a pure Zn overlayer, and $N_{\text{Zn}}=0$ to the pristine CdTe sample.

Finally, we have to derive values for the attenuation length $\lambda_M(E_X)$ within the matrix M . Generally, our consid-

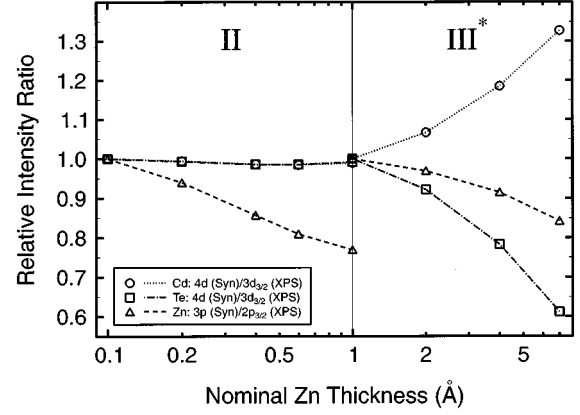


FIG. 11. Results of a model calculation for the relative intensity ratios of phase II and of a modified phase III*, calculated for the nominal Zn coverages of the experimental results of Fig. 13. Details of the model are described in the text.

erations are based on the curve for inelastic mean free path given by Seah and Dench³² by assuming a universal value $\lambda_{\text{univ.}} = \lambda_{\text{CdTe}}$, and hence a constant density of valence electrons [these values are given in Table I (Ref. 43)]. In phase II, however, the density of valence electrons is increased according to our model of additional Zn atoms within the CdTe matrix. We thus assumed an inverse linear dependence of the attenuation length λ on the atomic densities of Cd, Zn, and Te, as is consistent with the linear dependence of the ionization cross-section on the electronic density:⁴⁴⁻⁴⁶

$$\lambda(E_X, z) = \lambda_{\text{CdTe}}(E_X) \frac{2}{N_{\text{Cd}}(z) + N_{\text{Te}}(z) + N_{\text{Zn}}(z)}. \quad (3)$$

This ansatz ignores both distortions of the lattice in case of a Cd-Zn exchange due to different atomic radii, and the fact that a Cd-Zn exchange will decrease the overall electron density, while the valence electron density will be more or less unchanged. Note that the attenuation length $\lambda(E_X, z)$ to be used for the RIR calculation is now dependent on the z -position of the photoemitting atom.

The RIR evaluation for each phase of the Zn/CdTe interface formation is based on individual models for the atomic densities N_X , and thus also for $\lambda(E_X, z)$, because of Eq. (3). For the first phase of the interface formation, we assumed the formation of a pure Zn layer of a nominal thickness of 0.1 Å on top of the pristine CdTe surface. With this assumption, RIR values at 0.1 Å of 0.987 for Cd and 0.984 for Te are derived, i.e., only a small decrease occurs in both cases. In general, the RIR of a substrate element is reduced when an overlayer of a different material is deposited, since the overlayer affects the information depth of the surface-sensitive measurement more strongly than that of the bulk-sensitive measurement.

Results from the calculations for phases II and III are shown in Fig. 11. In phase II a reasonably good agreement with the experimentally observed RIR values can be obtained by starting with the 0.1-Å Zn-covered surface. Also, a constant Zn diffusion profile is assumed, with a constant fraction of Zn atoms up to a variable diffusion depth in addition to the Cd atoms of the pristine CdTe matrix (no Cd reduction, no Zn atoms beyond the diffusion depth). This

leads to a decrease in attenuation length within the Zn diffusion depth according to Eq. (3), thus influencing the information depth of all photoelectrons by an amount determined by the position of their emitter atoms. For the results shown for phase II in Fig. 11, we added one Zn atom per 15 Cd atoms within a diffusion depth determined by the nominal Zn thickness. For example, the maximum Zn diffusion depth for 1 Å Zn is then ≈ 30 Å. With these assumptions we find a significant reduction of the Zn RIR and a constancy of the Cd and Te RIR, in agreement with the experimental results of Fig. 10. The values of the Zn RIR can be modified by varying the overlayer thickness (derived from phase I), the fraction of in-diffused Zn atoms, the attenuation lengths, and the diffusion profile, while the overall trend remains unchanged. This finding further supports our interpretation of the second phase, in which Zn atoms diffuse into the CdTe surface region without changing the Cd concentration significantly (e.g., by occupying Cd vacancies and other defect sites).

In phase III, we assumed a replacement of Cd by Zn atoms throughout the maximum diffusion depth of phase II, followed by a segregation of Cd atoms. The Zn diffusion depth was held constant for increasing nominal Zn coverage in order to separate the influences of Cd segregation from the effects already discussed in phase II. This, of course, does not fully correspond to the proposed model for the interface formation, for which a further increase of the Zn diffusion depth would be expected for increasing Zn coverage (we thus denote the results of this simplified calculation as ‘‘phase III*’’). A more valid description can, however, be reached by qualitatively combining the results for phase II with those for phase III*. For phase III*, sum rules were applied in order to determine the fraction of Cd atoms being replaced by Zn and forced to the surface. As shown in Fig. 11, the Cd RIR is significantly increased in phase III*, while both the Te and Zn RIR are reduced. While the Cd RIR increase in both, the calculations and the experiment is thus regarded as a direct consequence of the Cd-Zn exchange and the Cd segregation, the reduction of Te and Zn is due to the formation of an additional overlayer of a different material. Thus the attenuation for Te is stronger than for Zn, since the difference in the attenuation lengths is larger in the Te case. In the case of Cd desorption or of Cd migration into the bulk of the sample, a reduced increase of the Cd RIR is derived, while the general trend remains unaltered.

As stated above, the behavior of phase III* is likely to be more realistic when the results of phase III* are combined with those of phase II, i.e., with a decrease in Zn RIR and a constancy for Cd and Te due to further indiffusion of Zn atoms. Thus the decrease of the Zn RIR in phase III* is actually steeper, in accordance with our experimental results.

The experimental evolution of the Te RIR, in contrast, cannot be explained on the basis of our simple Cd-Zn exchange model. We believe that this discrepancy is due to additional Te segregation, as has been frequently encountered in noble-metal/(Hg)CdTe and Mn/Cd(Zn)Te interfaces.^{20,47–51} In the latter case, the in-diffusing Mn atoms are expected to replace Cd atoms (just as in our case of Zn/CdTe), so that a Te segregation would not have been expected *a priori*, but nevertheless is unambiguously ob-

served. Thus we conclude that an additional Te segregation is feasible in our case as well, which is indirectly supported by the results of the calculation for phase III*. The fact that the increase in the Te RIR in Fig. 10 is significantly smaller than for the Cd RIR suggests that the amount of segregating Te atoms is significantly smaller than that of segregating Cd atoms.

VI. SUMMARY

Mg $K\alpha$ and synchrotron photoemission experiments have been combined to study the interface formation of Zn/CdTe(100). Five different phases have been distinguished for increasing Zn coverage by valence- and core-level binding-energy shifts, peak area investigations, and surface core-level shifts. Based on simple calculations of the attenuation of photoemission intensities, an interdiffusion model has been proposed.

In the first phase, adsorbed Zn atoms passivate surface defects, as can be derived from the band-bending behavior and from the surface core-level shifts. In phase II, Zn atoms diffuse into the CdTe matrix, occupying lattice sites, presumably by passivating Cd vacancy defects, and by forcing Cd atoms into interstitial sites. This finding is inferred from the Zn line position and the attenuation behavior of all photoemission peaks with increasing Zn coverage. Phase III is characterized by further Zn indiffusion and surface segregation of Te atoms and, predominantly, of Cd atoms being replaced by Zn. Moreover, Zn atoms are presumably located in interstitial sites, as judged from the Zn line position. By comparison of the binding-energy shifts of several spectral features, we arrive at a simple method of distinguishing between the formation of a Cd(Zn)Te compound (phase II) and the onset of surface segregation (phase III), which is associated with a sharp downward band bending. The formation of metallic islands and a metallic overlayer with simultaneous indiffusion of Zn is subdivided into phase IV, in which a metal-induced band bending is observed, leading to a surface photovoltage effect (SPV), and phase V, in which the detection of a Fermi edge gives direct proof of this SPV effect. Moreover, a further Cd species is detected in phase V, that can be correlated with segregated Cd in a metallic surrounding.

These findings suggest an elegant way to tailor the electronic structure of Cd(Zn)Te(100) surfaces by indiffusion of Zn atoms into CdTe in a near-surface region. Within this region we expect the Zn atoms to passivate both surface and bulk defects, while the compound semiconductor Cd(Zn)Te is formed. The onset of segregation marks the end of the formation process of a well-defined Cd(Zn)Te(100) surface with maximal Zn content. Since this onset is easily detected by a sharp increase in band bending, the indiffusion of Zn presents an easy, *in situ* method to optimize semiconductor heterojunctions involving Cd(Zn)Te as a substrate material.

ACKNOWLEDGMENTS

We would like to thank the BESSY staff for technical support. Financial support by the Deutsche Forschungsgemeinschaft through SFB 410 is gratefully acknowledged.

- ¹A. Wall, A. Raisanen, G. Haugstad, L. Vanzetti, and A. Franciosi, *Phys. Rev. B* **44**, 8185 (1991).
- ²H. Petersen, C. Jung, C. Hellwig, W. B. Peatman, and W. Gudat, *Rev. Sci. Instrum.* **66**, 1 (1995).
- ³According to the INSPEC data base (Institution of Electrical Engineers, last update 25 Aug. 1996), only one photoemission study of Zn adsorption on semiconductors has been performed by Raju *et al.* for Zn/CdSnAs₂, where the formation of an intermediate compound between Zn and As is proposed: D. V. R. Raju, V. J. Rao, S. Badrinarayanan, A. B. Mandale, and S. K. Kulkarni, *Appl. Phys. A: Solids Surf.* **50**, 339 (1990).
- ⁴H. Neureiter, S. Spranger, M. Schneider, U. Winkler, M. Sokolowski, and E. Umbach, *Surf. Sci.* **388**, 186 (1997).
- ⁵C. Heske, U. Winkler, R. Fink, E. Umbach, Ch. Jung, P. R. Bressler, and Ch. Hellwig, in *The Physics of Semiconductors*, edited by M. Scheffler and R. Zimmermann (World Scientific, Singapore, 1996), p. 823.
- ⁶C. Heske, U. Winkler, H. Neureiter, M. Sokolowski, R. Fink, E. Umbach, Ch. Jung, and P. R. Bressler, *Appl. Phys. Lett.* **70**, 1022 (1997).
- ⁷C. Heske, U. Winkler, G. Held, R. Fink, E. Umbach, Ch. Jung, P. R. Bressler, and Ch. Hellwig, *Phys. Rev. B* **56**, 2070 (1997).
- ⁸*Handbook of Thin Film Technology*, edited by L. I. Maissel and R. Glang (McGraw-Hill, New York, 1983), pp. 1–17.
- ⁹J. R. Chelikowsky and M. L. Cohen, *Phys. Rev. B* **14**, 556 (1976).
- ¹⁰Y. R. Wang, C. B. Duke, K. O. Magnusson, and S. A. Flodström, *Surf. Sci.* **205**, L760 (1988).
- ¹¹K. O. Magnusson, S. A. Flodström, and P. E. S. Persson, *Phys. Rev. B* **38**, 5384 (1988).
- ¹²H. Höchst, D. W. Niles, and I. Hernandez-Calderon, *Phys. Rev. B* **40**, 8370 (1989).
- ¹³D. W. Niles and H. Höchst, *Phys. Rev. B* **43**, 1492 (1991).
- ¹⁴D. W. Niles and H. Höchst, *Phys. Rev. B* **46**, 1498 (1992).
- ¹⁵K. U. Gawlik, J. Brüggemann, S. Harm, C. Janowitz, R. Manzke, M. Skibowski, C.-H. Solterbeck, W. Schattke, and B. A. Orlovski, *Acta Phys. Pol. A* **82**, 355 (1992).
- ¹⁶K.-U. Gawlik, J. Brüggemann, S. Harm, C. Janowitz, R. Manzke, and M. Skibowski, in *The Physics of Semiconductors*, edited by Ping Jiang and Hou-Zhi Zheng (World Scientific, Singapore, 1992), p. 485.
- ¹⁷K. U. Gawlik, J. Brüggemann, S. Harm, C. Janowitz, R. Manzke, M. Skibowski, C.-H. Solterbeck, W. Schattke, and B. A. Orlovski, *Acta Phys. Pol. A* **82**, 355 (1992).
- ¹⁸M. Alonso, R. Cimino, and K. Horn, *Phys. Rev. Lett.* **64**, 1947 (1990).
- ¹⁹M. H. Hecht, *Phys. Rev. B* **41**, 7918 (1990).
- ²⁰C. Heske, U. Winkler, R. Fink, E. Umbach, Ch. Jung, and P. R. Bressler, *Phys. Rev. B* **56**, 2085 (1997).
- ²¹K. C. Prince, G. Paolucci, V. Cháb, M. Surman, and A. M. Bradshaw, *Surf. Sci.* **206**, L871 (1988).
- ²²C. J. Vesely and D. W. Langer, *Phys. Rev. B* **4**, 451 (1971).
- ²³*Electronic Structure of Solids: Photoemission Spectra and Related Data*, edited by K. H. Hellwege and O. Madelung, Landolt-Börnstein, New Series, Group III, Vol. 23, Pt. a (Springer, Berlin, 1989), p. 81.
- ²⁴N. J. Shevchik, J. Tejeda, M. Cardona, and D. W. Langer, *Phys. Status Solidi B* **59**, 87 (1973).
- ²⁵W. Chen, A. Kahn, P. Soukiassian, P. S. Mangat, J. Gaines, C. Ponzoni, and D. Olego, *Phys. Rev. B* **51**, 14 265 (1995).
- ²⁶D. W. Niles and H. Höchst, *Appl. Phys. Lett.* **64**, 1147 (1994).
- ²⁷F. J. Himpsel, D. E. Eastman, E. E. Koch, and A. R. Williams, *Phys. Rev. B* **22**, 4604 (1980).
- ²⁸S.-H. Wei and Alex Zunger, *Phys. Rev. B* **37**, 8958 (1988).
- ²⁹The small amount of Zn encountered in the pristine CdTe sample of the second series does not influence the interpretations derived throughout this paper, since all features of the Zn/CdTe interface formation could be reproduced in the first series, for which no Zn was detected in the pristine CdTe sample.
- ³⁰*Structure Data of Elements and Intermetallic Phases*, edited by K.-H. Hellwege and O. Madelung, Landolt-Börnstein, New Series, Group IV, Vol. 6, Pt. a (Springer, Berlin, 1971), p. 409.
- ³¹In all three cases, one would expect a core-level shift similar to the shift observed between Cd in CdTe and in Cd metal, which is reported to be less than or equal to 0.2 eV toward lower binding energies [C. D. Wagner, in *Practical Surface Analysis*, 2nd ed., edited by D. Briggs and M. P. Seah (Wiley, Chichester, 1990), Vol. 1, p. 595]. In our case, the detected shift is significantly larger, but large deviations of this value can be expected due to doping-induced differences of the Fermi energy position within the semiconductor band gap.
- ³²M. P. Seah and W. A. Dench, *Surf. Interface Anal.* **1**, 2 (1979).
- ³³C. J. Powell, *Surf. Sci.* **299/300**, 34 (1994), and references therein.
- ³⁴W. H. Gries, *Surf. Interface Anal.* **24**, 38 (1996).
- ³⁵M. Vos, S. G. Anderson, and J. H. Weaver, *Phys. Rev. B* **39**, 3274 (1989).
- ³⁶J. H. Tregilgas and B. E. Gnade, *J. Appl. Phys.* **55**, 588 (1984).
- ³⁷E. P. Zucker, A. Hashimoto, T. Fukunaga, and N. Watanabe, *Appl. Phys. Lett.* **54**, 564 (1989).
- ³⁸M. Wada, M. Seko, K. Sakakibara, and Y. Sekiguchi, *Jpn. J. Appl. Phys.* **28**, L1700 (1989).
- ³⁹G. D. Watkins, *J. Cryst. Growth* **159**, 338 (1996).
- ⁴⁰J. Bollmann, M. Wienecke, J. Röhrich, and H. Kerkow, *J. Cryst. Growth* **159**, 384 (1996).
- ⁴¹Note that the segregated Cd atoms are in a different electronic surrounding than the Cd atoms of the terminating Cd layer; thus no increase in the surface-shifted component of, e.g., the Cd 3d_{3/2}, core levels would *a priori* be expected in this case.
- ⁴²M. P. Seah, in *Practical Surface Analysis* (Ref. 31), p. 224.
- ⁴³We are aware that the “universal curve” is a crude empirical approximation and that more accurate—but less “universal”—λ data are available (see, e.g., Refs. 33 and 34). However, the simplest possible choice of λ here is justified by the simplicity of the model and the fact that too little is known about the system and hence many assumptions are required (see text).
- ⁴⁴H. Bethe, *Ann. Phys. (Leipzig)* **5**, 325 (1930).
- ⁴⁵M. Gryzinski, *Phys. Rev.* **138**, A336 (1965).
- ⁴⁶W. Lotz, *Z. Phys.* **232**, 101 (1970).
- ⁴⁷G. D. Davis, W. A. Beck, N. E. Byer, R. R. Daniels, and G. Margaritondo, *J. Vac. Sci. Technol. A* **2**, 546 (1984).
- ⁴⁸G. D. Davis, N. E. Byer, R. A. Riedel, and G. Margaritondo, *J. Appl. Phys.* **57**, 1915 (1985).
- ⁴⁹A. Franciosi, P. Philip, and D. J. Peterman, *Phys. Rev. B* **32**, 8100 (1985).
- ⁵⁰D. J. Friedman, G. P. Carey, I. Lindau, and W. E. Spicer, *Phys. Rev. B* **34**, 5329 (1986).
- ⁵¹D. J. Friedman, I. Lindau, and W. E. Spicer, *Phys. Rev. B* **37**, 731 (1988).